Submitted to: Journal of Colloid and Interface Science

Title: Real-time observation of aortic vessel dilation through delivery of sodium nitroprusside via slow release mesoporous nanoparticles

Authors: Asima FAROOQ [1], Lubomira TOSHEVA[1], May AZZAWI [2]*, Debra WHITEHEAD [1]*.

1, Division of Chemistry and Environmental Science, Faculty of Science and Engineering, Manchester Metropolitan University, Manchester, M1 5GD, UK. Emails a.farooq@mmu.ac.uk; d.whitehead@mmu.ac.uk ; l.tosheva@mmu.ac.uk

2, School of Healthcare Science, Faculty of Science and Engineering, Manchester Metropolitan University, Manchester, M1 5GD, UK, Email: m.azzawi@mmu.ac.uk

Corresponding authors:

* Dr. Debra Whitehead, Tel +44 161 247 3341, Email d.whitehead@mmu.ac.uk

* Dr. May Azzawi, Tel +44 0161 247 3332, Email m.azzawi@mmu.ac.uk

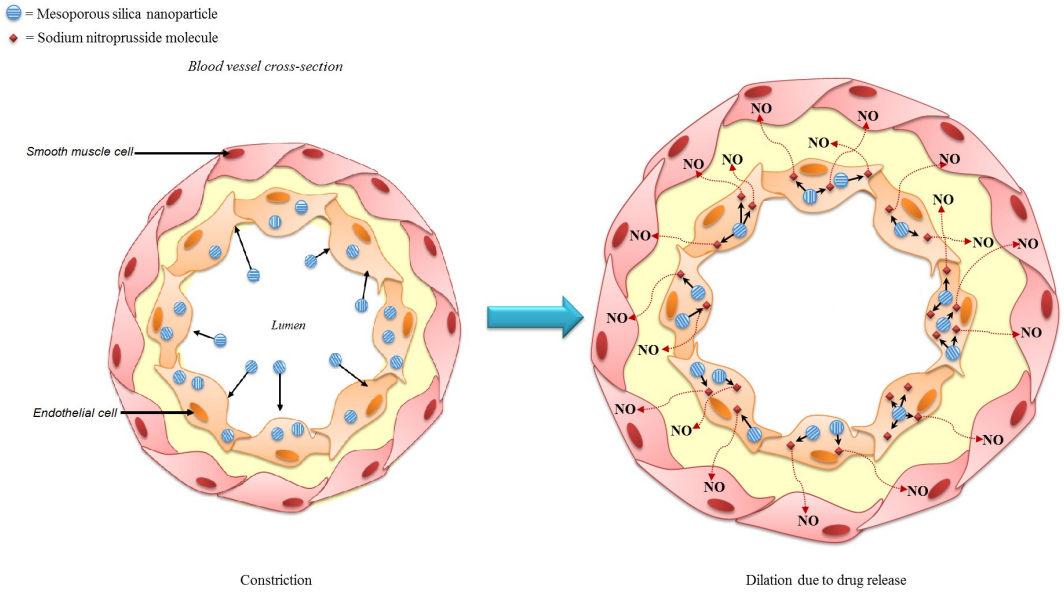

Abstract

Spherical mesoporous nanoparticles (MNPs) with a diameter of ~100 nm were synthesised via a sol-gel method in the presences of organic template (with and without fluorescein dye encapsulation). The template molecules were removed by acidic extraction to form a regular pore lattice structure. The nanoparticle size and morphology were analysed using transmission electron microscopy and dynamic light scattering analysis. The MNPs were further characterised by zeta potential, nitrogen adsorption measurements and infra-red spectroscopy. The interior pores had an average diameter of ~3 nm and were loaded with an endothelial-independent vasodilator, sodium nitroprusside (SNP). The optimal drug loading and drug release was determined in high potassium physiological salt solution using dialysis and atomic absorption spectroscopy. We demonstrate that the initial instantaneous release is due to the surface desorption of the drug followed by diffusion from the pores. Furthermore, these drug loaded MNPs (with and without fluorescein dye encapsulation) were added to viable aortic vessels and release in real-time was observed, *in-vitro*. MNPs and loaded with and without SNP were incubated with the vessel (at 1.96×10^{12} NP mL^{-1}) over a 3 h time period. The real-time exposure to unloaded MNPs resulted in a small attenuation in constriction that occurred after approximately 1 h. In contrast, MNPs loaded with SNP led to a rapid relaxation of aortic vessels that was sustained over the 3 h period ($p<0.001$).

Keywords:
Mesoporous nanoparticles, sodium nitroprusside, drug release, aortic vessels, vascular function, vasodilator.

1. Introduction

Progress in nanoparticle fabrication techniques has enabled the tailoring of nanoparticle properties for the development of innovatively designed biological drug delivery vehicles [1-3]. Orally and intravenously administered drugs circulate throughout the body and may have a number of systemic side effects, often leading to poor efficiency of the drug [4]. Consequently, there is a drive for the development of new drug delivery systems. In particular, mesoporous nanoparticles (MNPs) can be fabricated using colloidal methods with small diameters that are able to enter cells. Regular pore structure is produced during the surfactant template synthesis method [5]. The resulting MNPs have high surface to volume ratio's with pore channels that can be loaded with guest molecules. The exterior surface is available for functionalisation to enable targeted therapy of intracellular structures [6]. Furthermore, these particles have been used for diagnostic imaging and cellular localisation by confocal microscopy and flow cytometry by incorporation of fluorescent dye molecules within the MNPs silica framework [7]. Once the nanoparticles have been drug loaded, the release is governed by constrained pore diffusion enabling these particles to be utilised for slow drug release applications [8, 9]. Previous studies have used MNPs as hosts (such as MCM-41and SBA-15) and loaded with guest molecules (such as drugs, enzymes, DNA and luminescent dyes) to produce effective systems in which the host-guest interaction plays a vital role in their application [10].

The ordered pore network of MNPs allows fine control of the drug loading and release kinetics, while the large surface area allows adsorption of the required dosage of drug [5]. Release kinetics has been demonstrated from MNPs using luminescent molecules and ibuprofen [9, 11-14]. One study showed that 80 % of ibuprofen was

released after only 50 min from MNPs with pore size of 3.4 nm and particle diameter of 50 μm [15]. Another study demonstrated that it took 31 h for the release of 60 % of ibuprofen loaded into MNPs (diameter 950 nm and pore size of 2.5 nm). There has been an abundance of studies showing that MNPs are internalised into the cytoplasm of mammalian cells with low cytotoxicity (LD_{50} values greater than 1mg mL^{-1}) demonstrating their biocompatibility [16].

The aortic vessel is the largest artery in vertebrates and plays an important role in the transport of blood and the maintenance of blood pressure (Fig. 1). Arteries are comprised of three layers, an endothelial layer facing the lumen, a smooth muscle layer, and an outer adventitial layer [17]. Vessel viability and the integrity of the endothelial and smooth muscle cell layers can be verified by examining vascular responses to vasodilator and vasoconstrictor agonists [18]. A major vasodilator released naturally by endothelial cells is nitric oxide (NO) and is important in the maintenance of vessel diameter. Reduced bioavailability of NO has been demonstrated in a number of vascular related conditions, including diabetes and hypertension [19]. The development of nanoparticles that can deliver sustained and controlled release of NO could have enormous impact on human health. One approach has been the development of silica hydrogel nanoparticle matrices, whereby the entrapped NO molecules are released when exposed to moisture [20]. Sodium nitroprusside (SNP) is an endothelial independent vasodilator that causes relaxation of the smooth muscle cells by delivery of NO, which is a labile ligand, contained within the SNP molecular complex [21-23]. In this study, we report for the first time the *in vitro* real-time vasodilator action of SNP on arterial vessels delivered via

MNPs. Controlled release of SNP from MNPs is a promising avenue for the development of therapeutic intervention in cardiovascular disease.

2. Materials and methods

2.1. Materials

Fluorescein isothiocyanate (FITC), (3-aminopropyl)trimethoxysilane (APTMS), tetraethyl orthosilicate (TEOS), hydrochloric acid (HCl, 37 %) and sodium nitroprusside (SNP) were purchased from Sigma-Aldrich. Hexadecyltrimethyammonium bromide (CTAB), anhydrous dimethylformamide (DMF), sodium hydroxide (NaOH) and methanol (MeOH) were purchased from Fisher-Scientific. Salt solutions were prepared using sodium chloride (NaCl), potassium chloride (KCl), magnesium sulphate heptahydrate ($MgSO_4.7H_2O$), potassium phosphate monobasic (KH_2PO_4), calcium chloride ($CaCl_2.2H_2O$), ethylenediaminetetraacetic acid dipotassium salt dihydrate ($K_2EDTA.2H_2O$) purchased from Fisher-Scientific.

Physiological Salt Solution (PSS) was prepared using the following chemical composition [mM]: 119 NaCl, 4.7 KCl, 1.2 $MgSO_4.7\ H_2O$, 25 $NaHCO_3$, 1.17 KH_2PO_4, 0.03 $K_2EDTA.2H_2O$, 5.5 glucose and 1.6 $CaCl_2.2H_2O$; *pH* 7.4. Potassium Physiological Salt Solution (KPSS) was prepared using the following chemical composition [mM]: 78.2 NaCl, 60 KCl, 1.2 $MgSO_4.7\ H_2O$, 25 $NaHCO_3$, 1.17 KH_2PO_4, 0.03 $K_2EDTA.2H_2O$, 5.5 glucose and 1.6 $CaCl_2.2H_2O$; *pH* 7.4 as previously described by Farooq et al [24].

2.2. Synthesis of non-dye encapsulated mesoporous nanoparticles

Mesoporous silica nanoparticles (MNPs) were synthesised using a modified template directed self-assembly method published by *Slowing et al* without the

incorporation of FITC dye molecules [25]. Briefly, anhydrous DMF (5 mL) was mixed with APTMS (50 μL). CTAB (1 g) was dissolved in H_2O (480 mL) and 2 M NaOH solution (3.5 mL) was added and stirred at 80 °C. TEOS (4 mL) was added followed by the addition of the APTMS mixture (500 μL). The resulting mixture was stirred vigorously at 80 °C for 2 h producing an opaque white suspension. The MNPs were collected and washed with MeOH by centrifugation (14,000 rpm/ 15 min) several times. The surfactant template (CTAB) was extracted from the as-synthesised product by refluxing the product in MeOH (200 mL) and concentrated HCl (2 mL) for 24 h. The MNPs were washed using the same procedure as before. The acid extraction step was repeated twice.

2.3. Synthesis of dye encapsulated mesoporous nanoparticles

Fluorescein isothiocyanate encapsulated mesoporous nanoparticles (FITC MNPs) were synthesised via the same method as the MNPs except that FITC (2.5 mg) was added to the mixture of anhydrous DMF and APTMS and then stirred for 3 h. [25]. The resulting product was a yellow suspension.

2.4. Characterisation of mesoporous nanoparticles

The MNPs hydrodynamic size and zeta potential were determined by dynamic light scattering (DLS) and laser Doppler velocimetry respectively (Malvern Zetasizer nano ZS instrument). The zeta potential was determined for MNPs in both distilled water and KPSS. The MNP sizes were further confirmed using scanning electron microscopy (SEM, JEOL 5600LV SEM) and transmission electron microscopy (TEM, Philips

Technai^{TM} 12 Biotwin TEM). Nitrogen adsorption isotherms at -196 °C were measured with a Micromeritics ASAP 2020 instrument. Samples were degassed at 200 °C for 12 h prior to analysis. The Brunauer-Emmett-Teller (BET) surface area was calculated in the range of relative pressures 0.03-0.05 (p/ p^o). The pore size distributions were determined by the Barrett-Joyner-Halenda (BJH) method from the desorption branch of the isotherms. The infra-red analysis was used for confirmation of template removal (Nicolet Avatar 360 FT-IR). Fluorescence spectroscopy was used to determine the encapsulation of dye molecules within the MNPs by producing a calibration plot of know concentrations of FITC dye molecules (Hitachi fluorescence spectrophotometer F-2500).

2.5. Drug loading efficiency

Drug loading efficiency was calculated using equation 1 below [26]. 250 mg of MNPs with and without dye molecules were suspended into 25 mL of the SNP methanol solution (1×10^{-5} mol dm^{-3}) and stirred for 48 h to facilitate drug uptake. The solution was centrifuged to separate the nanoparticles loaded with SNP. The supernatant was analysed using inductively coupled plasma atomic emission spectroscopy (ICP-AES) to measure concentration of Fe as a single atom is present per SNP molecule. The loading efficiency percentage was calculated as the ratio of difference between the initial drug concentration and the drug concentration in the supernatant (free drug) to the initial drug concentration, as followed

Drug loading efficiency (%) = Total drug-[Free drug] [Total drug] x 100 **(1)**

2.6. Release profile of sodium nitroprusside from mesoporous nanoparticles

For the release profile, MNPs-SNP (128 mg) was dispersed in 4 mL of KPSS and placed in small vial and covered with dialysis tubing on the top. The resulting vial was placed in a glass bottle containing KPSS (15 mL) with the dialysis membrane immersed in the solution. The release of SNP was examined by taking 1 mL aliquots of the solution contained within the beaker and replacing the solution with 1 mL of KPSS at regular time intervals. This process was repeated for FITC MNPs under the same conditions. The concentration of SNP within the aliquots was quantified by measuring the concentration of Fe with ICP-AES. Initially, the method was validated by ascertaining linearity of standard curves; five standard curves of known concentrations (3.4×10^{-8}, 1.7×10^{-7}, 3.4×10^{-7}, 1.7×10^{-6}, 3.4×10^{-6} mol dm^{-3}) of SNP in diluted KPSS (1:5 ratio of KPSS to water) were calibrated. The stability of the auto-sampler was established with five replicates of each sample.

2.7. Vascular functional studies

The thoracic aortic arteries of male Wistar rats were used for the *in vitro* studies (n=13 animals; one vessel from each animal). The rats of approximately 150-250 g weight were humanly killed by stunning followed by cervical dislocation following institutional approval and in accordance with guidelines issued by the European Commission Directive 86/609/EEC. The perivascular adipose tissue was removed from the vessel while being gassed (95 % O_2: 5 % CO_2) in cold PSS, as it can attenuate contraction. The vessels was dissected into 3-4 mm aortic rings and mounted in an organ

bath system filled with PSS solution (35 ºC) by threading the rings between a U-shaped hook and ascending wire attached to a micrometer, Fig. 2. The tension between the two wires was recorded using Labchart 6 (Powerlab, AD Instruments, UK**)**. The aortic rings were placed under a constant 2 g tension throughout the experimentation as preliminary results have determined this to be the optimal tension value. Vessels were equilibrated for approximately 1 hour, followed by pre-constriction with high K^+ (60 mM, KCl) to test vessel viability and achieve stable contraction, as previously described by Farooq et al [24]. Responses to SNP were examined by adding cumulative doses of SNP (0.01-100 μM) as a control. MNPs (1.96×10^{12} NP mL^{-1}) and FITC MNPs (1.96×10^{12} NP mL^{-1}) were incubated with constricted vessels over a 3 h period. The number of nanoparticles per mL was determined by calculating the volume and density of a sphere with a diameter of 100 nm and finally the mass of a mesoporous nanoparticle; the density of mesoporous silica was 0.814 g cm^{-3}[27].

2.8. Release of sodium nitroprusside from mesoporous nanoparticles in vitro

The effect of the SNP loaded MNPs and FITC MNPs was examine by addition of 1.96×10^{12} NP mL^{-1} to preconstricted vessels using the approach described above.

2.9. Transmission electron microscopy

Vessels tested in the release studies were fixed immediately after the functional studies, using 2.5 % glutaraldehyde in 0.1 M sodium cacodylate buffer (pH 7.3) for 2 h at

22 ˚C. The samples were postfixed with reduced osmium (OsO_4 1 % + $K_4Fe(CN)_6$ 1.5 %) for 1 h, then dehydrated in a series of alcohols, infiltrated with TAAB LV resin and polymerized for 24 h at 60 ˚C, as previously described (Akbar *et al*. [28]). Ultrathin 70 nm sections were cut with Leica 'Ultracut S' ultramicrotome and placed on formvar carbon coated TEM copper grids (Agar Scientific). The samples were observed using a Tecnai 12 Biotwin TEM at 80 kV as previously described by Farooq *et al.* [24].

2.10. Statistical analysis

Data are expressed as mean ± standard error of mean (S.E.M.) with 'n' representing the number of vessels. Dilator responses are expressed as percent relaxation. Concentration response curves were assessed using statistical package for the social sciences (SPSS; version 19). The difference between groups at a given concentration was tested by one way analysis of variance (ANOVA) with Bonferroni corrections. Statistical significance is taken as $P<0.05$ as previously described by Farooq et al [24].

3. Results and discussion

3.1. Mesoporous silica nanoparticles

The SEM images in Fig. 3 confirm that particles produced have a narrow size distribution with an average diameter of 95±13 nm for MNPs (Fig. 3A) and 109±18 nm for the FITC MNPs (Fig. 3B). The TEM images showed that the MNPs (Fig. 4A) and FITC MNPs (Fig. 4B) were mainly spherical in shape with some variation in the size distributions. The particles had regular, parallel-aligned pore channels confirming the successful removal of the template using the acid extraction method. DLS measurements showed that the average hydrodynamic diameter of the as-synthesised MNPs was 182.9 nm and the FITC MNPs was 183.9 nm with a polydispersion index of 0.49 and 0.4 respectively (Table 1). A polydispersity index larger than 0.1 indicates the presence of aggregated particles. This would explain the large differences between the sizes determined by TEM and DLS. In addition, it is well known that the size determined by DLS is overestimated compared to size determined by TEM. Equally the zeta potential measurement for colloidal stability for particles to remain individual should be no less than -30mV, -13.8 demonstrates that there is potential for aggregation. The template extracted MNPs and FITC MNPs were stable in water and high potassium salt solution (KPSS) as demonstrated with the zeta potential measurements (Table 1, Fig. S1). Furthermore, when template extracted MNPs were placed in KPSS the hydrodynamic diameter increased to 247.3 nm from 182.9 nm with the zeta potential values increasing to -13.8 mV from -30.0 mV, higher ionic strength solution leads to a smaller electrical double layer thickness, weaker electrostatic repulsive force, and subsequently larger hydrodynamic size. Similar behaviour was shown for the FITC MNPs in KPSS media

with the average hydrodynamic diameter increasing to 227.8 nm from 183.9 nm, along with the increase in the zeta potential values to -15.6 mV from –30.0 mV.

The Fourier transform infra-red (FTIR) spectroscopy confirms that the CTAB template has been successfully removed (Fig. 5), as the characteristic two sharp peaks of the organic surfactant at 2853 cm^{-1} and 2923 cm^{-1} were diminished.

The amount of dye molecules encapsulated within the silica framework of the MNPs was quantified with fluorescence spectroscopy. The fluorescence spectra of known concentrations of FITC were used to produce a calibration graph (Fig. S2). The excitation wavelength of FITC is 490 nm with an emission at 520 nm. The dye molecules encapsulated within the MNP were quantified by analysing the amount of dye molecules within the supernatant after centrifugation from the reaction media. Thus, the dye concentration within the MNPs was calculated by subtracting the concentration within the supernatant from the actual concentration of dye used (Table 2). The mass of FITC dye molecules within FITC MNPs was determined to be 2.48 mg. The FITC MNPs demonstrated a strong fluorescent signal (Fig. S3).

The nitrogen adsorption and desorption of the MNPs follows the general Langmuir isotherm trend of mesoporous materials (Fig. 6) indicating monolayer adsorption of gas within the capillaries of the pores. From the gas adsorption analysis it was possible to determine that the silica MNPs have a pore diameter of 2.9 nm as shown in the pore size distribution graph (insert in Fig. 6A). The overall surface area was determined as 853.3 ± 9.0 m^2g^{-1} confirming successful synthesis of high porosity particles. FITC MNPs has a surface area of 1154.5±2.1 m^2g^{-1}, which is larger than the silica MNPs, while the insert confirm the pore size to be 2.8 nm, similar to the silica

MNPs (Fig. 6B). All the isotherms indicate that ordered mesopores are present in the samples (the step at ~0.4 p/ p^o).

3.2. Sodium nitroprusside release from mesoporous nanoparticles

The concentration of SNP was calculated from iron concentration which originated from the SNP drug and is shown in Table 3. The drug loading efficiency of the MNPs was determined to be 86.30 % whilst for the FITC MNPs it was 96.46% for 250mg of the particles, indicating that nearly all the SNP drug was adsorbed when soaked in a concentration of 1×10^{-5} mol dm^{-3} SNP. There was a higher amount of drug adsorption by the FITC MNPs as there may be residual amine functional groups from the dye coupling reaction causing electrostatic attraction of SNP on the pore surface.

The release rate of SNP from MNPs and FITC MNPs was investigated (Fig. 7). The time course of SNP release demonstrates that there is a rapid initial release for both types of MNPs over 10 min, this is expected due to the large concentration gradient but also due to some desorption on the particle exterior surface. From 10 min to 180 min there is a shallow gradient in the graph indicating slow release.

3.3. Detection of mesoporous nanoparticles within vascular tissue

In the present study, we demonstrate that the exposure of viable aortic vessels to MNPs and FITC MNPs of approximately 100 nm leads to their internalisation into the cytoplasm of the endothelial cells that line aortic vessels as shown in the TEM cross

section image in Fig.8. No particles were observed in the nucleus of the cells, elastic lamina, smooth muscle or adventitial layers.

3.4. Sodium nitroprusside release from mesoporous nanoparticles in vitro

MNPs and FITC MNPs at 1.96×10^{12} NP mL^{-1} concentration were placed in the organ-bath system. The trend observed for the vasodilation of aortic vessels when incubated in MNPs loaded with SNP led to a significant reduction in constriction (Fig. 9). Furthermore, the constriction level was sustained for the control over a 3 h period. The real-time exposure of aortic vessels to FITC MNPs at 1.96×10^{12} NP mL^{-1} has a similar observable constriction level as the control over a 3 h time period (Fig. 10). The FITC MNPs loaded with SNP leads to a rapid relaxation of aortic vessels however, the relaxation was sustained over 120 min, thereafter followed by re-constriction. The statistical analysis confirms that the relaxation is significant for the SNP loaded FITC MNPs (Table 4).

The dosage of MNPs added to the aortic vessels was 1.96×10^{12} NP mL^{-1} was the same concentration used in our previous study in which we tested non-porous silica nanoparticles (71±6 nm) [24]. In line with our previous observations with non-porous silica nanoparticles, the MNPs and FITC MNPs had no detriment to the endothelial-independent vasodilation indicating good biocompatibility. This is in good agreement with the literature where human cervical cancer cells (HeLa) were exposed to 100 µg mL^{-1} of FITC MNPs and no difference between the control and the FITC MNPs cell growth profile were shown thus confirming they are not cytotoxic [25].

Data from the *in vitro* real-time release studies were used to construct percentage relaxation graphs to SNP from MNPs (shown in Fig. 9B). There was no statistically significant difference over the 3 h exposure time period between the KPSS control and high concentration of MNPs (Table 4). Furthermore, the exposure of viable aortic vessels to MNPs loaded with SNP led to a rapid relaxation of the vessels. The MNPs loaded with SNP led to an initial sharp release of SNP within the first 20 min leading to 57.74 % relaxation. The maximum relaxation was 77.08 % and was reached at 125 min.

Similarly, for the percentage relaxation graphs of MNPs, there was no statistically significant affect over the 3 h exposure time period between the KPSS control and FITC MNPs (Fig. 11B). Also, the MNPs loaded with SNP, led to a rapid relaxation of the vessels. The FITC MNPs loaded with SNP led to an initial sharp release of SNP within the first 20 min leading to 61.93 % relaxation. The maximum relaxation was 64.16 % and was reached at 35 min.

In order to calculate the SNP release in real-time under physiological conditions, a calibration plot of known concentrations of SNP against relaxation was constructed (Fig. 11). The logarithm equation, determined from the calibration plot, allowed for the calculation of SNP concentration released at a given time (Table 5). The calculated SNP release from the MNP with and without dye estimated from the calibration plot using the *in vitro* studies showed that the concentration of SNP after 180 minutes was similar to the release study in the dialysis tubing supernatant determined with atomic absorption spectroscopy (Table 6). There was a lower concentration *in vitro* which is expected as the relaxation occurs from the dissociation of the NO ligand from the SNP, which diffuses through to the smooth muscle cells of the vessel.

4. Conclusions

In conclusion, we have designed a drug delivery system allowing the release of a model drug - sodium nitroprusside (SNP agonist) from the mesoporous matrix. MNPs with an average size of 100 nm were used in the experiments in pure form or after encapsulation of a fluorescein isothiocyanate dye (FITC MNPs). The drug-loaded particles were added to isolated aortic vessels to record the real-time release profile, ex vivo. Vessel relaxation was evident over a 3 h duration of the incubation period for both MNPs and FITC MNPs. We have created a biocompatible slow release drug delivery vehicle that can deliver sustained and controlled release of SNP. SNP delivers NO which acts on the smooth muscle cells causing vasodilation and is currently utilised in clinical practice to treat hypotension. These particles possess great potential as a novel drug delivery platform for therapeutic applications in the future for treatment of cardiovascular disease, particularly in preventing SNP overdose, which can be very dangerous for patients. Furthermore, FITC labelling of the MNPs could enable simultaneous imaging and therapy in the future.

Acknowledgements

Financial support from the Dalton Research Institute, MMU, is gratefully acknowledged. The authors would also like to thank Dr. Aleksander Mironov (The University of Manchester), for his assistance with the TEM analysis. **References**

[1] C.J. Kirkpatrick, W. Bonfield, NanoBioInterface: a multidisciplinary challenge, J. R. Soc. Interface 7 (2010) S1-S4.

[2] D. Knopp, D. Tang, R. Niessner, Bioanalytical applications of biomolecule-doped nanometer-sized silica particles, Analytica Chemica Acta 647 (2009) 14-30.

[3] M. De, P.S. Ghosh, V.M. Rotello, Applications of nanoparticles in biology, Advanced Materials 20 (2008) 4225-4241.

[4] Z.-Z. Li, L.-X. Wen, L. Shao, J.-F. Chen, Fabrication of porous hollow silica nanoparticles and their applications in drug release control, J. Controlled Release 98 (2004) 245-254.

[5] M. Vallet-Regi, F. Balas, D. Arcos, Mesoporous materials for drug delivery, Angewandte Chemie International Edition, 46 (2007) 7548-7558.

[6] Z. Tao, B.B. Toms, J. Goodisman, T. Asefa, Mesoporosity and functional group dependent endocytosis and cytotoxicity of silica nanomaterials, Chemical Research in Toxicology 22 (2009) 1869-1880.

[7] M.-C. Estévez, M.B. O'Donoghue, X. Chen, W. Tan, Highly fluorescent dye-doped silica nanoparticles increase flow cytometry sensitivity for cancer cell monitoring, Nano. Res. 2 (2009) 448-461.

[8] J. Gu, W. Fan, A. Shimojima, T. Okubo, Organic-inorganic mesoporous nanocarriers integrated with biogenic ligands, Small 3 (2007) 1740-1744.

[9] I.I. Slowing, J.L. Vivero-Escoto, C.-W. Wu, S.-Y. Lin, Mesoporous silica nanoparticles as controlled release drug delivery and gene transfection carriers, Advanced Drug Delivery Reviews, 60 (2008) 1278-1288.

[10] H. Ritter, J.H. Ramm, D. Brühwiler, Influence of the stuctural properties of mesoporous silica on the adsorption of guest molecules, Materials 3 (2010) 4500-4509.

[11] G. Wang, A.N. Otuonye, E.A. Blair, K. Denton, Z. Tao, T. Asefa, Functionalized mesoporous materials for adsorption and release of different drug molecules: a comparative study, J. Solid State Chem. 182 (2009) 1649-1660.

[12] Y.N. Zhao, B.G. Trewyn, I.I. Slowing, V.S.Y. Lin, Mesoporous silica nanoparticle-based double drug delivery system for glucose-responsive controlled release of insulin and cyclic AMP, J. Am. Chem. Soc. 131 (2009) 8398-8400.

[13] J.M. Rosenholm, M. Linden, Towards establishing structure-activity relationships for mesoporous silica in drug delivery applications, J. Controlled Release 128 (2008) 157-164.

[14] W. Xu, Q. Gao, Y. Xu, D. Wu, Y. Sun, W. Shen, F. Deng, Controllable release of ibuprofen from size-adjustable and surface hydrophobic mesoporous silica spheres, Powder Technology 191 (2009) 13-20.

[15] C. Charnay, S. Be´gu, C. Tourne´-Pe´teilh, L. Nicole, D.A. Lerner, J.M. Devoisselle, Inclusion of ibuprofen in mesoporous templated silica: drug loading and release property, European J. Pharmaceutics and Biopharmaceutics 57 (2004) 533–540.

[16] Z. Tao, Y. Xie, B.B. Toms, J. Goodisman, T. Asefa, Mesoporosity and Functional Group Dependent Cytotoxicity of Silica Nanomaterials, Chem. Res. Toxicol. 22 (2009) 1869-1880

[17] O. Mirea, I. Donoiu, I.E. Pleşea., Arterial aging: a brief review, Rom. J. Morphol. Embryol. 53 (2012) 473-477.

[18] M. Azzawi, C. Austin, Extravascular pressure modulates responses of isolated rat coronary arteries to vasodilator, but not vasoconstrictor stimuli, Am. J. Physiol. Heart Circ. Physiol. 290 (2006) H1151-H1156.

[19] Z. Bagi, A. Koller, G. Kaley, Superoxide-NO interaction decreases flow- and agonist-induced dilations of coronary arterioles in Type 2 diabetes mellitus, Am. J. Physiol. Heart. Circ. 285 (2003) H1404-H1410.

[20] A.J. Friedman, G. Han, M.S. Navati, M. Chacko, L. Gunther, A. Alfieri, J.M. Friedman, Sustained release nitric oxide releasing nanoparticles: characterization of a novel delivery platform based on nitrite containing hydrogel/glass composites, Nitric Oxide 19 (2008) 12-20.

[21] J.N. Bates, M.T. Baker, R.Jr. Guerra, D.G. Harrison, Nitric oxide generation from nitroprusside by vascular tissue. Evidence that reduction of the nitroprusside anion and cyanide loss are required, Biochemical pharmacology 42 (1991) S157-S165.

[22] K.F Ricardo, S.M. Shishido, M.G. de Oliveira, M.H. Krieger, Characterization of the hypotensive effect of S-nitroso-N-acetylcysteine in normotensive and hypertensive conscious rats, Nitric Oxide 7 (2002) 57-66.

[23] F. PeÂrez-VizcaõÂno, A.L. Cogolludo, F. ZaragozaÂ-ArnaÂez, S. Fajardo, M. Ibarra, J.G. LoÂpez-LoÂpez, J. Tamargo, Vasodilator effects of sodium

nitroprusside, levcromakalim and their combination in isolated rat aorta, British J. Pharmacology 128 (1999) 1419-1426.

[24] A. Farooq, D. Whitehead, M. Azzawi, Attenuation of endothelial-dependent vasodilator responses, induced by dye-encapsulated silica nanoparticles, in aortic vessels, Nanomedicine 0 (2013) 1-12.

[25] I. Slowing, B.G. Trewyn, V.S.-Y. Lin, Effect of surface functionalization of MCM-41-type mesoporous silica nanoparticles on the endocytosis by human cancer cells, JACS 128 (2006) 14792-14793.

[26] M.H. Mashhadizadeh, M. Amoli-Diva, Drug-carrying amino silane coated magnetic nanoparticles as potential vehicles for delivery of antibiotics, J. Nanomed. and Nanotechnol. 3 (2012) 1-7.

[27] H. Meng, M. Wang, H. Liu, X. Liu, A. Situ, B. Wu, Z. Ji, C. H. Chang, and A. E. Nel, Use of a lipid-coated mesoporous silica nanoparticle platform for synergistic gemcitabine and paclitaxel delivery to human pancreatic cancer in mice. ACS nano 9, 4 (2015) 3540-3557.

[28] N. Akbar, T. Mohamed, D. Whitehead, M. Azzawi, Biocompatibility of amorphous silica nanoparticles: Size and charge effect on vascular function, in vitro, Biotechnol. Appl. Biochem. 58 (2011) 353-362.

FIGURE CAPTION

Figure 1: Graphical illustration of a cross-section of the aortic vessel.

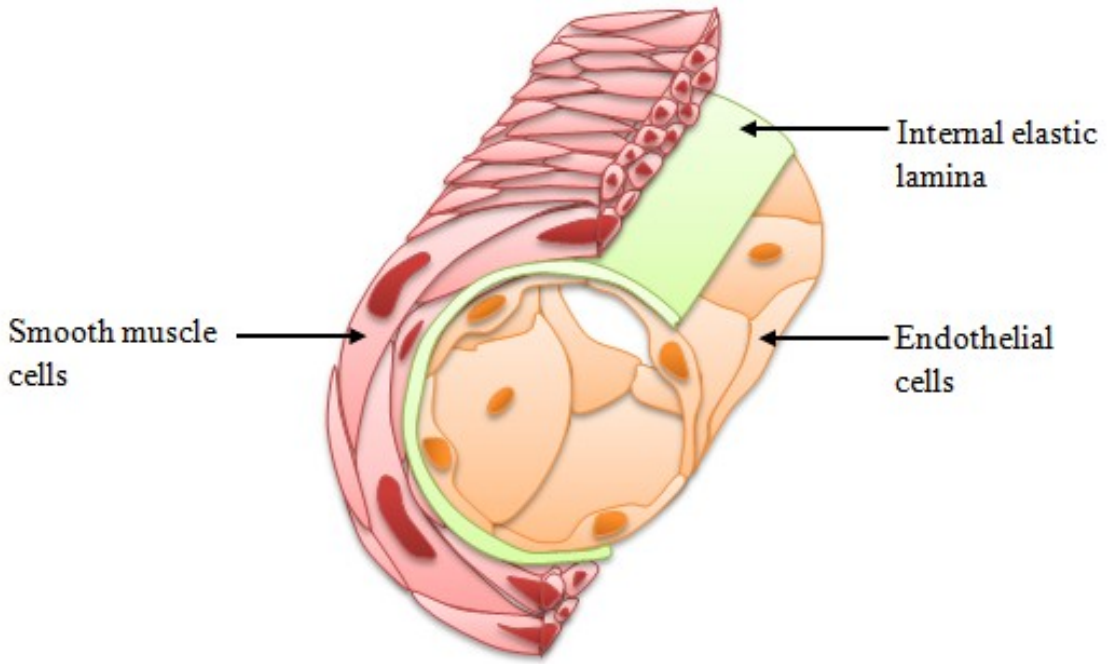

Figure 2: Scanning electron microscope image of A) mesoporous nanoparticles and B) fluorescein isothiocyanate encapsulated mesoporous nanoparticles.

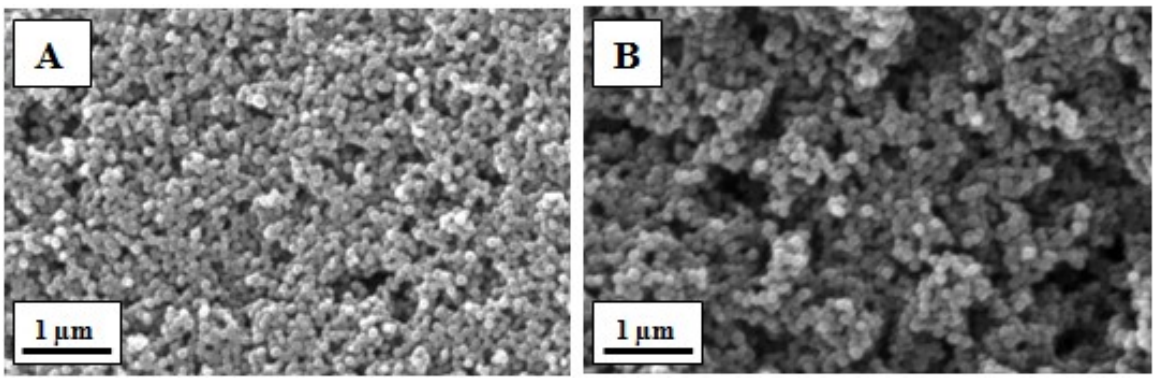

Figure 3: Transmission electron microscope image of A) mesoporous nanoparticles, B) side-view of the mesopore channels and C) front-view of the mesopores.

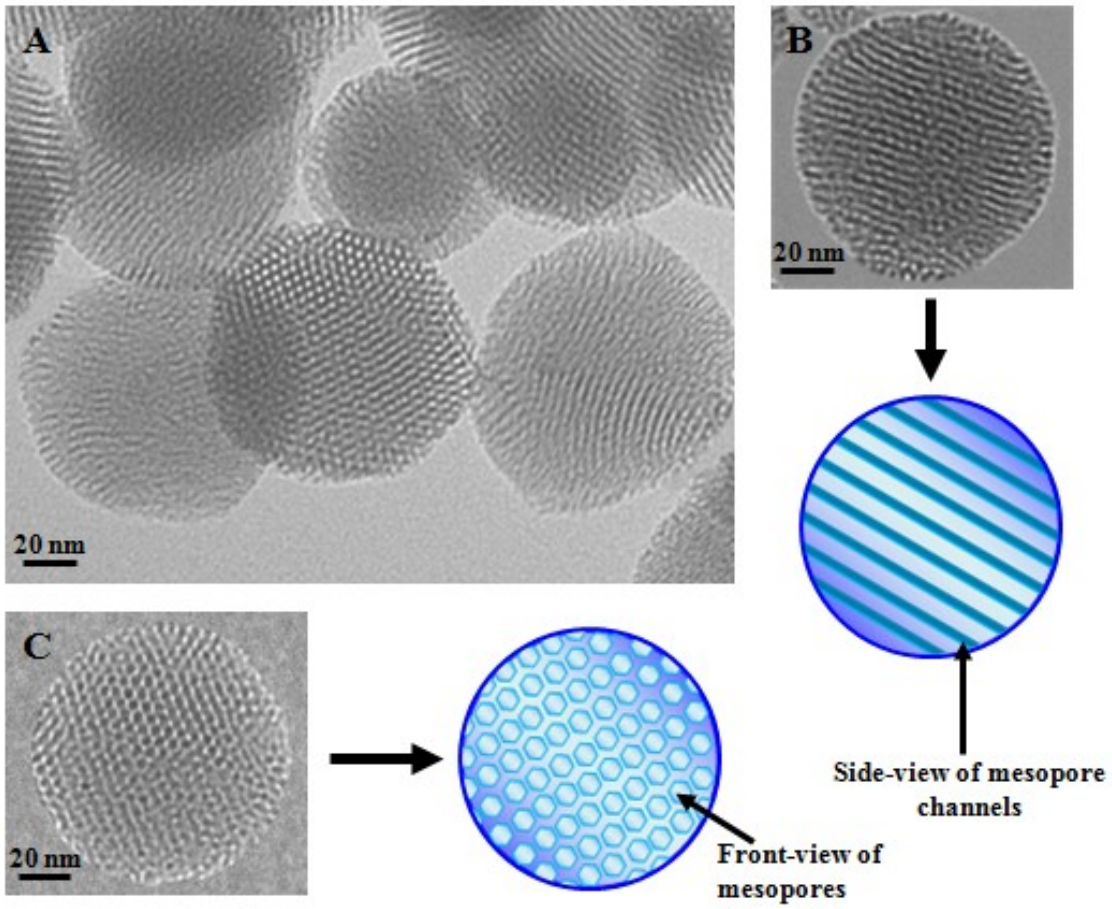

Figure 4: FTIR spectra of A) MNP and B) FITC MNP, where the solid lines represent template intact and dashed are template removed.

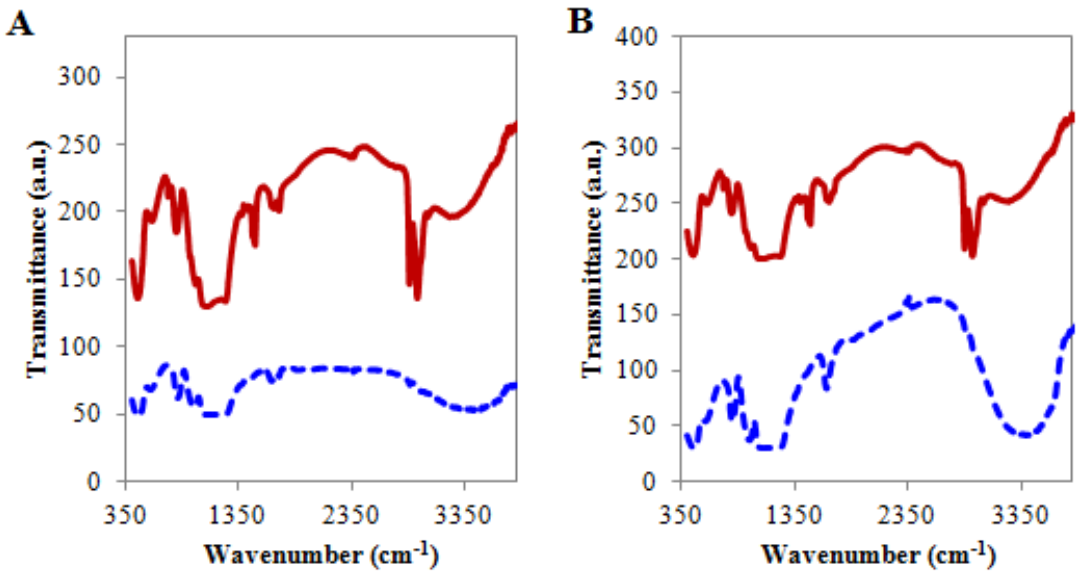

Figure 5: Nitrogen sorption isotherm for gas adsorption (diamond curve) and desorption (circle curve) of A) mesoporous nanoparticles and B) fluorescein isothiocyanate mesoporous nanoparticles.

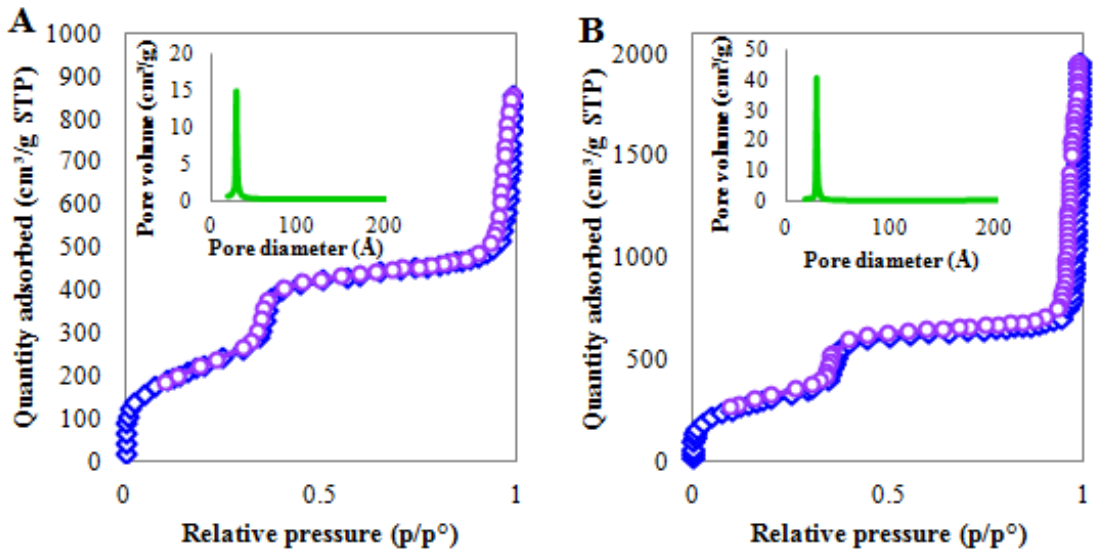

Figure 6: Schematic illustration of the interaction between sodium nitroprusside and the mesopore channel.

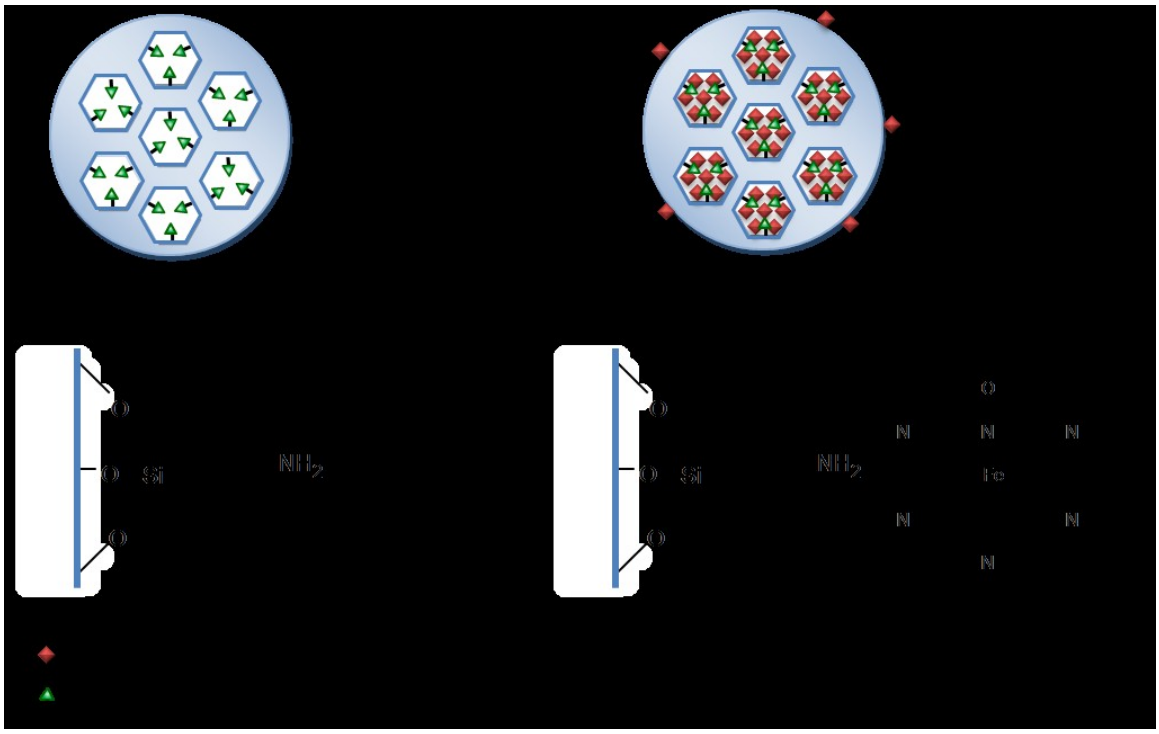

Figure 7: Release profile of sodium nitroprusside from mesoporous nanoparticles using atomic absorption spectroscopy.

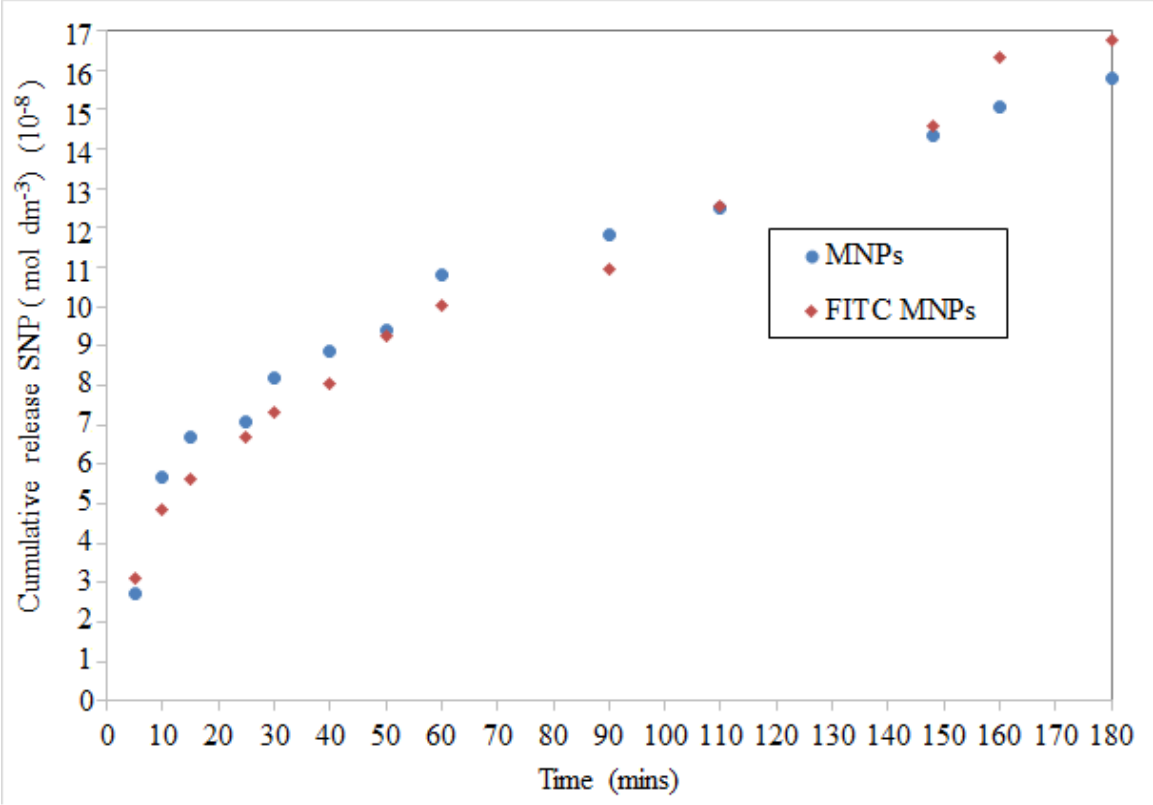

Figure 8: TEM images of sections of fixed aortic vessels after incubation with a) mesoporous silica nanoparticles and b) fluorescein isothiocyanate incorporated mesoporous silica nanoparticles.

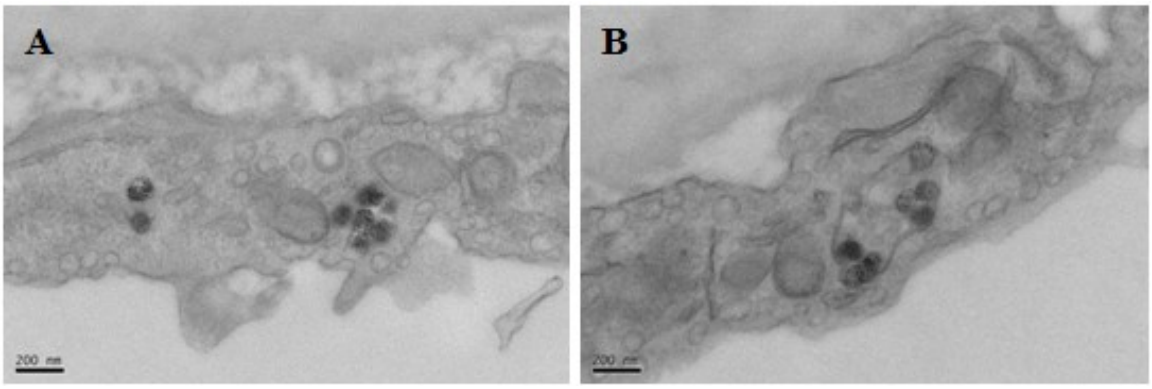

Figure 9: The influence of sodium nitroprusside loaded mesoporous nanoparticles at A) high concentration on constricted aortic vessels in real-time. B) The influence of sodium

nitroprusside loaded mesoporous nanoparticles on endothelium-independent vasodilator responses. 'n' is number of vessels.

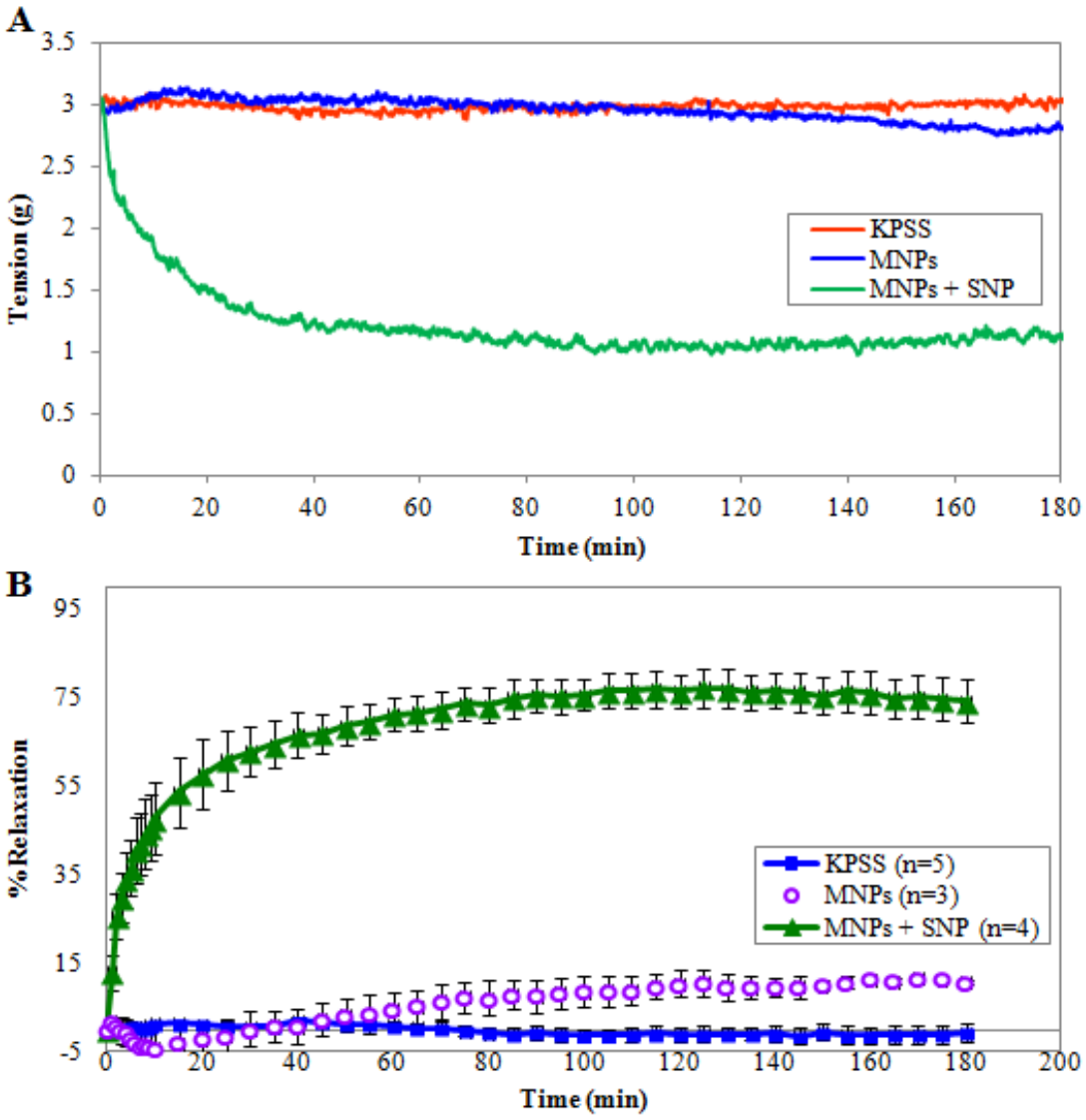

Figure 10: The influence of sodium nitroprusside loaded FITC mesoporous nanoparticles at A) high concentration on constricted aortic vessels in real-time. B) The influence of sodium nitroprusside loaded fluorescein isothiocyanate encapsulated mesoporous nanoparticles on endothelium-independent vasodilator responses. 'n' is number of vessels.

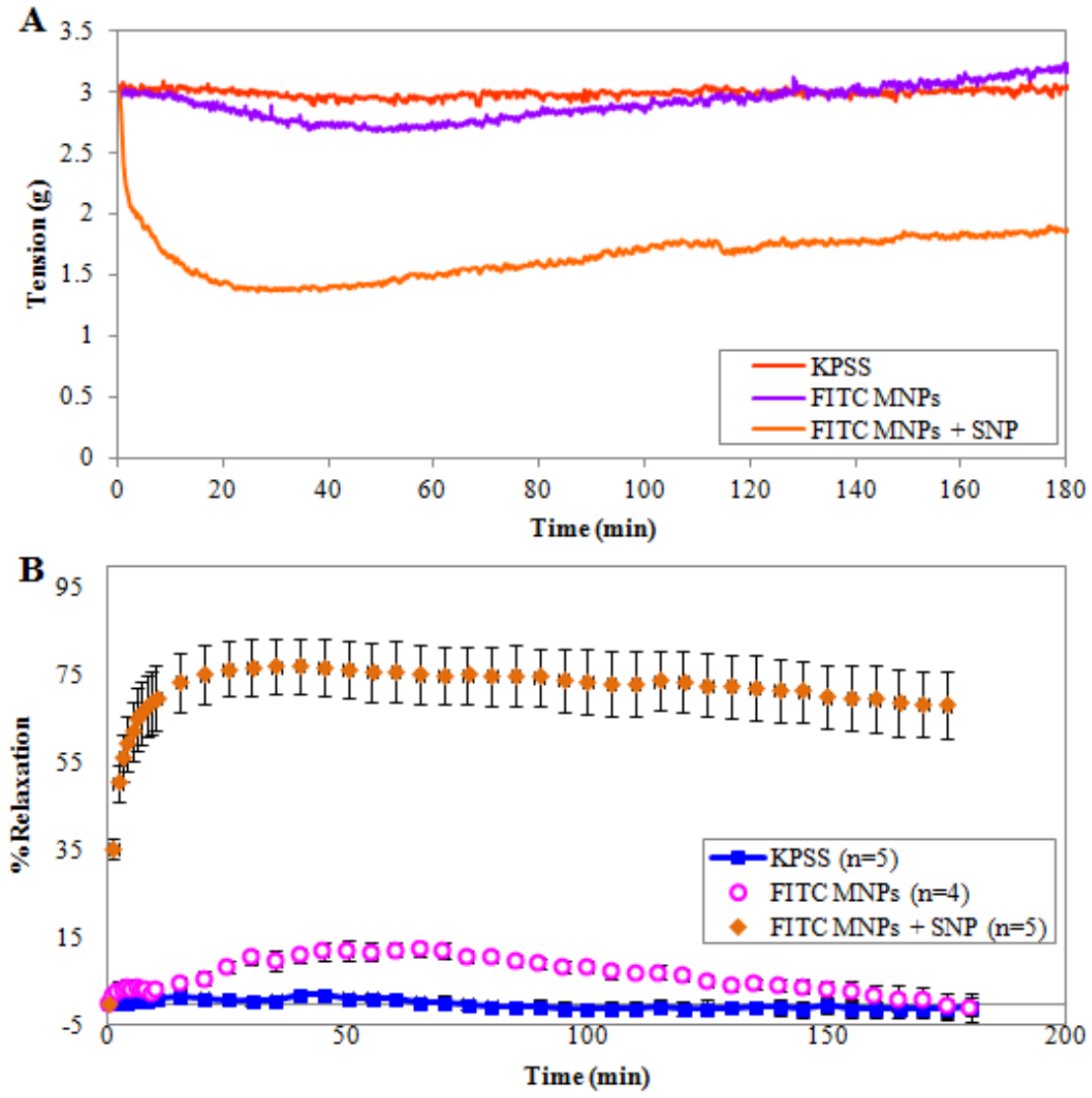

Figure 11: Calibration spectra of endothelium-independent vasodilator response against known concentrations of sodium nitroprusside.

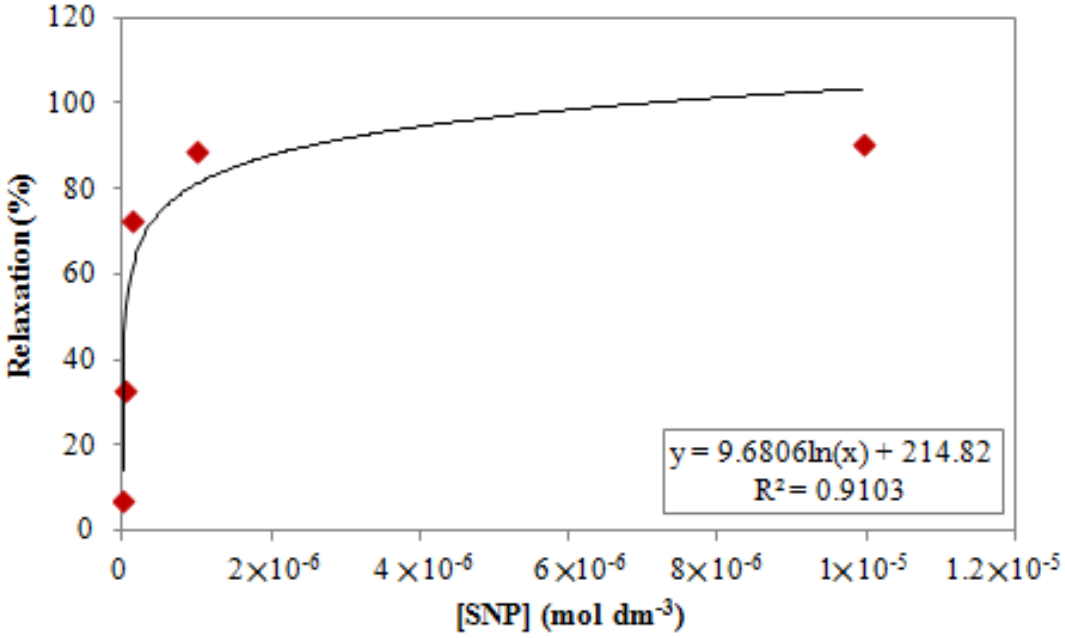
120
100
80
60
40
20
0
Relaxation (%)
0
2×10-6
4×10-6
6×10-6
8×10-6
1×10-5
1.2×10-5
[SNP] (mol dm-3)
y = 9.6806ln(x) + 214.82
R² = 0.9103

TABLE 1: Hydrodynamic size and stability measurements of mesoporous nanoparticles, in water and high potassium physiological salt solution.

Nanoparticles type	Primary diameter [a] (nm)	Hydrodynamic diameter [b] (nm)		ζ potential (mV)	
		In water	*In KPSS*	*In water*	*In KPSS*
MNPs	95±13	182.9	247.3	-30.0	-13.8
FITC MNPs	109±18	183.9	227.8	-30.0	-15.6

[a] Mean (±SD) diameter determined by SEM.
[b] ***Mean PCS measurement.***

TABLE 2: Quantification of dye molecules within the nanoparticles.

	Fluorescence intensity (a.u.)	Dye concentration (mol dm^{-3})	Moles of Dye (mol)	Mass of dye (mg)
FITC MNPs supernatant	44.48	9.94×10^{-8}	4.63×10^{-8}	1.80×10^{-2}
FITC MNPs	7866	2.62×10^{-5}	6.36×10^{-6}	2.48

TABLE 3: Quantification of SNP molecules within the nanoparticles.

	[SNP] Soaking mol dm^{-3}	[SNP] Supernatant mol dm^{-3}	[SNP] loading mol dm^{-3}
MNPs	1×10^{-5}	0.137×10^{-5}	0.863×10^{-5}
FITC MNPs	1×10^{-5}	0.0354×10^{-5}	0.966×10^{-5}

TABLE 4: One-way Anova with Bonferroni correction for relaxation of aortic vessels due to incubation in MNP and MNP loaded SNP with and without dye encapsulation (where NS=not significant, *=p<0.05, **=p<0.01 and ***=p<0.001).

Time (min)	Significance difference in relaxation in comparison to KPSS control			
	MNPs	MNPs + SNP	FITC MNPs	FITC MNPs + SNP
1	NS	**	NS	***
2	NS	***	NS	***
3	NS	***	NS	***
4	NS	***	NS	***
5	NS	***	NS	***
6	NS	***	NS	***
7	NS	***	NS	***
8	NS	***	NS	***
9	NS	***	NS	***
10	NS	***	NS	***
15	NS	***	NS	***
20	NS	***	NS	***
25	NS	***	NS	***
30	NS	***	NS	***
35	NS	***	NS	***
40	NS	***	NS	***
45	NS	***	NS	***
50	NS	***	NS	***
55	NS	***	NS	***
60	NS	***	*	***
65	NS	***	*	***
70	NS	***	*	***
75	NS	***	*	***
80	NS	***	*	***
85	NS	***	*	***
90	NS	***	*	***
95	NS	***	NS	***
100	NS	***	NS	***
105	NS	***	NS	***
110	NS	***	NS	***
115	NS	***	NS	***
120	NS	***	NS	***
125	NS	***	NS	***
130	NS	***	NS	***
135	NS	***	NS	***
140	NS	***	NS	***
145	NS	***	NS	***
150	NS	***	NS	***
155	NS	***	NS	***
160	NS	***	NS	***
165	NS	***	NS	***
170	NS	***	NS	***
175	NS	***	NS	***
180	NS	***	NS	***

TABLE 5: The concentration of SNP released from the MNP matrix *in vitro*, calculated from the logarithmic equation derived from the SNP control relaxation calibration graph.

Time (min)	Concentration of SNP releases from the MNPs *in vitro*	Concentration of SNP releases from the FITC MNPs *in vitro*
1	8.82×10^{-10}	6.09×10^{-09}
2	3.25×10^{-09}	1.71×10^{-08}
3	5.08×10^{-09}	2.32×10^{-08}
4	7.62×10^{-09}	2.50×10^{-08}
5	1.00×10^{-08}	3.14×10^{-08}
6	1.52×10^{-08}	3.42×10^{-08}
7	1.75×10^{-08}	4.02×10^{-08}
8	2.19×10^{-08}	5.28×10^{-08}
9	2.57×10^{-08}	5.56×10^{-08}
10	3.17×10^{-08}	6.13×10^{-08}
15	5.84×10^{-08}	1.12×10^{-07}
20	8.97×10^{-08}	1.38×10^{-07}
25	1.23×10^{-07}	1.72×10^{-07}
30	1.52×10^{-07}	1.73×10^{-07}
35	1.77×10^{-07}	1.74×10^{-07}
40	2.19×10^{-07}	1.74×10^{-07}
45	2.33×10^{-07}	1.62×10^{-07}
50	2.76×10^{-07}	1.47×10^{-07}
55	3.05×10^{-07}	1.23×10^{-07}
60	3.60×10^{-07}	1.23×10^{-07}
65	3.76×10^{-07}	1.17×10^{-07}
70	4.04×10^{-07}	1.16×10^{-07}
75	4.62×10^{-07}	1.19×10^{-07}
80	4.44×10^{-07}	1.07×10^{-07}
85	5.21×10^{-07}	1.05×10^{-07}
90	5.63×10^{-07}	1.08×10^{-07}
95	5.50×10^{-07}	$8.35\times^{1008}$
100	5.67×10^{-07}	7.59×10^{-08}
105	6.22×10^{-07}	6.94×10^{-08}
110	6.20×10^{-07}	7.27×10^{-08}
115	6.52×10^{-07}	9.48×10^{-08}
120	6.16×10^{-07}	8.60×10^{-08}
125	6.62×10^{-07}	7.36×10^{-08}
130	6.53×10^{-07}	7.19×10^{-08}
135	6.01×10^{-07}	6.63×10^{-08}
140	$6.21\times^{-07}$	$6.67\times^{-08}$
145	$6.13\times^{-07}$	$7.23\times^{-08}$
150	$5.55\times^{-07}$	$5.74\times^{-08}$

155	$6.15\times^{-07}$	$5.54\times^{-08}$
160	$5.97\times^{-07}$	$5.27\times^{-08}$
165	5.28×10^{-07}	$4.86\times^{-08}$
170	$5.42\times^{-07}$	$4.86\times^{-08}$
175	$5.09\times^{-07}$	$4.64\times^{-08}$
180	$4.91\times^{-07}$	$4.51\times^{-08}$

TABLE 6: The total concentration of SNP released from the MNP matrix, *in vitro* after 180 mins.

	MNPs	FITC MNPs
Total SNP released in the *in vitro* study (mol dm^{-3})[α]	4.91×10^{-7}	0.451×10^{-7}
SNP released from MNP after (mol dm^{-3})[γ]	9.99×10^{-7}	1.66×10^{-7}

[α] Calculated from the in vitro control studies of SNP.
[γ] Determined from atomic absorption spectroscopy.